



The influence of Sm doping in the electron-doped manganites $\text{La}_{0.9}\text{Te}_{0.1}\text{MnO}_3$

G.H. Zheng^{a,b,*}, Z.X. Dai^{a,b}, Y.Y. Zhang^{a,b}, Y.P. Sun^{a,b}

^a School of Physics and Material Science, Anhui University, Hefei 230039, PR China

^b Key Laboratory of Materials Physics, Institute of Solid State Physics, Chinese Academy of Sciences, Hefei 230031, PR China

ARTICLE INFO

Article history:

Received 23 February 2009

Received in revised form

16 September 2009

Accepted 22 September 2009

Available online 30 September 2009

PACS:

67.55.Hc

74.25.Fy

Keywords:

Structural properties

Transport mechanism

ABSTRACT

The effect of Sm-doping on structural, magnetic and transport properties in the electron-doped manganites $\text{La}_{0.9-x}\text{Sm}_x\text{Te}_{0.1}\text{MnO}_3$ ($0 \leq x \leq 0.15$) with fixed carrier concentration is investigated. All samples show rhombohedral structure with the space group $R\bar{3}C$. Both the Curie temperature T_C and magnetization M of samples decrease with increasing Sm-doping level. For all samples, there exists two metal–insulator (M–I) transitions in the temperature dependence of the resistivity curves $\rho(T)$. The resistivity of the sample increases with increasing Sm-doping level. By fitting the $\rho(T)$ data in the high paramagnetic (PM) region, it is found that the transport properties are dominated by the small polaron conduction (SPC) mechanism. With increasing Sm-doping level, the polaron binding energy increases, which is ascribed to the lattice distortion due to the Sm doping.

© 2009 Elsevier B.V. All rights reserved.

1. Introduction

The $\text{A}_{1-x}\text{D}_x\text{MnO}_3$ perovskites manganites are interesting systems because of the anomalous magnetic and transport properties exhibited by them such as colossal magnetoresistance (CMR), metal–insulator (M–I) transition, antiferromagnetic–ferromagnetic (AFM–FM) ordering, and lattice dynamics associated with phase transitions [1–3]. Zener's double exchange (DE) interaction between Mn ions through charge carriers in the oxygen 2p orbitals was introduced in order to explain the coupling of magnetic and electronic properties in these compounds [4]. However, many studies have shown that DE interaction is not sufficient to explain the complex physics in these compounds, especially with regard to the lattice distortions coinciding with the emergence of CMR [5–7]. In addition, the phase separation [8] (PS) has also been suggested to play an important role.

In order to understand the unusual magnetic and transport properties of doped perovskites $\text{A}_{1-x}\text{D}_x\text{MnO}_3$, many studies have been carried out by doping the trivalent rare earth sites (A site) with divalent atoms (Ca, Sr, Ba, etc.) [9–11] or tetravalent atoms (Te, Zr, Ce) [12–14]. It has shown that the average ionic size of cations (R, A) [15,16], the size mismatch between R and A cations [17] contributes to the physical properties of this system. The study

of Hwang et al. [15] on $(\text{La}_{1-x}\text{R}_x)_{0.7}\text{Ca}_{0.3}\text{MnO}_3$ reveals that the T_C and the conductivity decrease when some La^{3+} is replaced by Pr^{3+} or Y^{3+} , in other words, the magnetic and transport properties of the system are a strong function of average A size ionic radius, $\langle r_A \rangle$. They have concluded that the electronic and magnetic state are highly relevant to a geometrical index called the Goldsmith tolerance factor t , which decides the crystallographic distortions from the cubic ($t=1$) perovskite structure. The Goldsmith tolerance factor, describing the stability of the perovskite structure, is defined as $t = (r_A + r_O) / \sqrt{2}(r_B + r_O)$. In such a definition, r_i ($i = \text{A, B, or O}$) represents the average ionic size of each element. With decreasing t , the Mn–O–Mn bond angle, to which the transfer integral is related and which describes the electron hopping between Mn^{3+} and Mn^{4+} , decreases. Therefore, in order to better understand the physical properties of the electron-doped manganites $\text{La}_{0.9}\text{Te}_{0.1}\text{MnO}_3$ with the change of the A-site ionic radii, we studied the effects of the partial substitution of Sm for La with fixed $\text{Mn}^{2+}/\text{Mn}^{3+}$ ratio at 1/9. The structure, resistivity ρ , magnetization M measurement results of $\text{La}_{0.9-x}\text{Sm}_x\text{Te}_{0.1}\text{MnO}_3$ ($0 \leq x \leq 0.15$) compound have been presented and discussed in this text.

2. Experimental

Polycrystalline samples with nominal compositions $\text{La}_{0.9-x}\text{Sm}_x\text{Te}_{0.1}\text{MnO}_3$ ($0 \leq x \leq 0.15$) were prepared by solid-state reaction method. Stoichiometric high-purity La_2O_3 , Sm_2O_3 , TeO_2 and MnO_2 powders were mixed and ground, and then heated in air at 750 °C for 24 h. The powder obtained was ground, pelletized, and sintered at 1100 °C for 24 h with three intermediate grinding, and finally, the furnace was cooled down to the room temperature. The structure and lattice constant were determined by powder X-ray diffraction using Cu $K\alpha$ radiation at

* Corresponding author at: School of Physics and Material Science, Anhui University, Hefei 230039, PR China.

E-mail address: ghzheng@issp.ac.cn (G.H. Zheng).

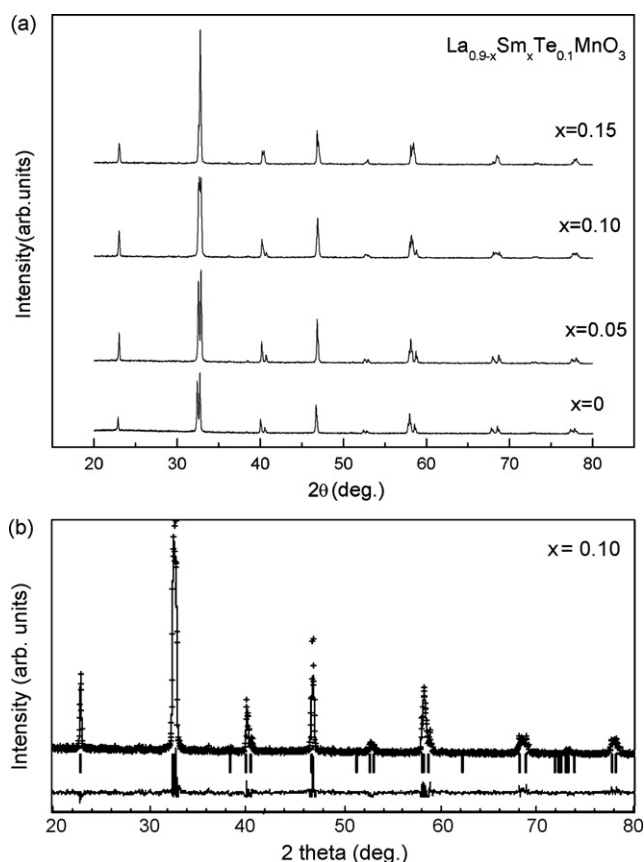


Fig. 1. (a) XRD patterns of $\text{La}_{0.9-x}\text{Sm}_x\text{Te}_{0.1}\text{MnO}_3$ ($0 \leq x \leq 0.15$) compounds at the room temperature. (b) The experimental and calculated XRD patterns of the sample with $x=0.10$. Crosses indicate the experimental data and the calculated data is continuous line overlapping them. The lowest curve shows the difference between experimental and calculated patterns. The vertical bars indicated the expected reflection positions.

the room temperature. The magnetic measurements were performed on a Quantum Design superconducting quantum interference device (SQUID) MPMS system ($1.8\text{ K} \leq T \leq 400\text{ K}$, $0\text{ T} \leq H \leq 5\text{ T}$). The temperature dependence of ρ was measured by the standard four-probe from 5 to 350 K at zero field in a commercial Quantum Design Physical Property Measurements System (PPMS) ($1.8\text{ K} \leq T \leq 400\text{ K}$, $0\text{ T} \leq H \leq 9\text{ T}$).

3. Results and discussion

3.1. Structural properties

Fig. 1a shows that X-ray diffraction patterns of $\text{La}_{0.9-x}\text{Sm}_x\text{Te}_{0.1}\text{MnO}_3$ ($0 \leq x \leq 0.15$) at room temperature. All the samples are single phase with no detectable secondary phases. XRD patterns for all samples can be indexed by rhombohedral lattice with the space group $R\bar{3}C$. The experimental and calculated XRD patterns for the sample with $x=0.10$ are presented in Fig. 1b. The structural parameters are refined by the standard Rietveld technique [18] and the fitting between the experimental spectra and the calculated values is relatively good based on the consideration of lower RP values as shown in Table 1.

Fig. 2a plots the Mn–O–Mn bond angle and Mn–O length extracted from the Rietveld refinement at room temperature. The Mn–O–Mn bond angle decreases with increasing the doping level x , whereas the Mn–O bond length increases which displays the inverse correlation to the variation in the Mn–O–Mn bond angle. It is well known that there are two possible origins of the lattice distortion of the perovskite structures: one is the deformation of the Mn^{3+}O_6 octahedra, originating from the Jahn–Teller (J–T)

Table 1
Refined structural parameters of $\text{La}_{0.9-x}\text{Sm}_x\text{Te}_{0.1}\text{MnO}_3$ ($0 \leq x \leq 0.15$) at room temperature.

Parameter	$x=0$	$x=0.05$	$x=0.10$	$x=0.15$
a (nm)	0.54761	0.54851	0.54862	0.54878
c (nm)	1.3228	1.3264	1.3265	1.3266
v (nm^3)	0.33025	0.33237	0.33660	0.33853
$d_{(\text{Mn}-\text{O})}$ (nm)	0.18401	0.18426	0.18505	0.18623
$\langle \text{Mn}-\text{O}-\text{Mn} \rangle$ ($^\circ$)	167.09	166.63	163.65	160.92
W	0.1176	0.1146	0.1113	0.1072
R_p (%)	9.04	8.38	8.01	8.99

effect which is decided by the concentration of Mn^{3+} ions, and the other is the variation of the average ionic radius of the A-site element (r_A). In the present samples, the concentration of Mn^{3+} is fixed and the lattice distortion is ascribed to the variation of the average A-site radius (r_A), induced by the substitution of smaller Sm^{3+} ($r=0.113\text{ nm}$) for larger La^{3+} ($r=0.122\text{ nm}$) ions. The exchange interaction between the Mn–Mn depends on the bond angle and the bond length. The increase of Mn–O length and decrease of Mn–O–Mn bond angle weaken the Mn–Mn exchange interaction, leading to a lower magnetic ordering temperature and a smaller magnetization magnitude value (see later discussion of M – T curves). At the same time, the reduction in Mn–O–Mn bond angle provides a local trap of e_g electrons, and then leads to the increase of resistivity and the activation energy of electron hopping (as discussed below).

The electronic bandwidth W has been used to discuss magnetic and transport properties of perovskites with varied A-site

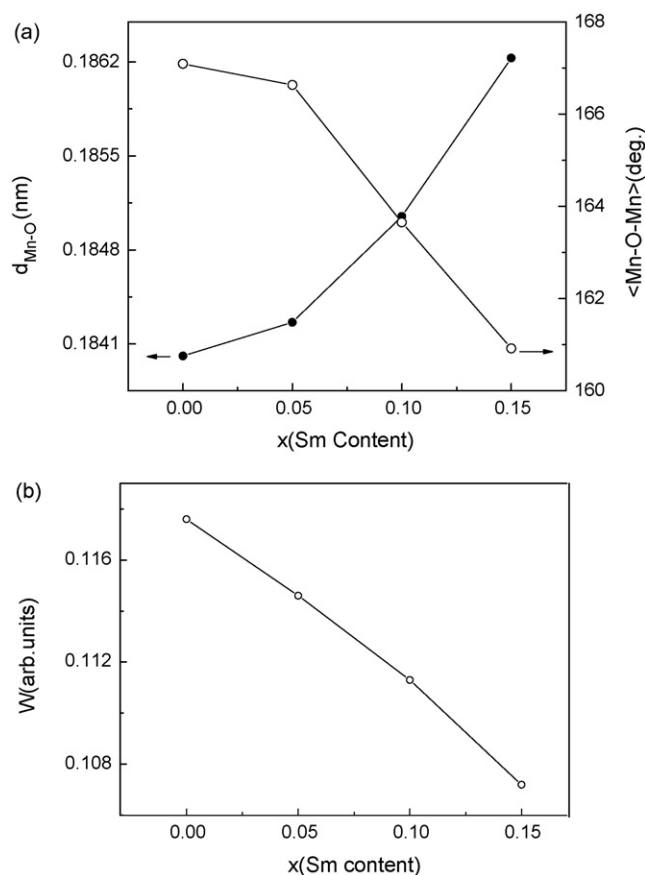


Fig. 2. (a) The Mn–O bond length and Mn–O bond angle for $\text{La}_{0.9-x}\text{Sm}_x\text{Te}_{0.1}\text{MnO}_3$ ($0 \leq x \leq 0.15$) as a function of the Sm concentration, determined from the room temperature XRD. (b) The electronic bandwidth for $\text{La}_{0.9-x}\text{Sm}_x\text{Te}_{0.1}\text{MnO}_3$ ($0 \leq x \leq 0.15$) as a function of the Sm concentration, determined from the room temperature XRD.

Download English Version:

<https://daneshyari.com/en/article/1620926>

Download Persian Version:

<https://daneshyari.com/article/1620926>

[Daneshyari.com](https://daneshyari.com)